

# MURMURATIONS, MESTRE–NAGAO SUMS, AND CONVOLUTIONAL NEURAL NETWORKS FOR ELLIPTIC CURVES

JOANNA BIERI, EDGAR COSTA, ALYSON DEINES, KYU-HWAN LEE, DAVID LOWRY-DUDA,  
THOMAS OLIVER, YIDI QI, AND TAMARA VEENSTRA

ABSTRACT. We apply one-dimensional convolutional neural networks to the Frobenius traces of elliptic curves over  $\mathbb{Q}$  and evaluate and interpret their predictive capacity. In keeping with similar experiments by Kazalicki–Vlah, Bujanović–Kazalicki–Novak, and Pozdnyakov, we observe high accuracy predictions for the analytic rank across a range of conductors. We interpret the prediction using saliency curves and explore the interesting interplay between murmurations and Mestre–Nagao sums, the details of which vary with the conductor and the (predicted) rank.

## 1. INTRODUCTION

The vanishing order of a rational  $L$ -function at its central point is a fundamental arithmetic invariant. For example, this vanishing order for the  $L$ -function associated with an abelian variety is expected to be equal to the rank of the finitely generated abelian group of rational points. Inspired partly by this connection to a mysterious arithmetic quantity, a recent theme in the literature has been to machine learn the vanishing order of a rational  $L$ -function from a finite list of (normalized) Frobenius traces indexed by primes [HLO23; KV23; HLOP24; Poz24; BBCDLLQV25a]. This body of work fits into a wider literature of machine learning arithmetic quantities including class numbers [HLO22a; AHLOS23], Galois groups [LL24], Tate–Shafarevich groups [BBFHS24] and Fricke signs [BBCDLLQV25b]. All told, it is well documented that standard machine learning algorithms can achieve high accuracy in predicting arithmetic quantities.

A more interesting, and more challenging, question is what to make of the apparent success of machine learning in this context. For example, can highly accurate arithmetic predictions be attributed to meaningful arithmetic structures, and can these structures be uncovered by interpreting how the predictions are made? A preliminary step in this direction led to the discovery of so-called *murmurations* [HLOP24]. Although originating from experimental work, murmurations are a genuinely number-theoretic phenomenon that can be studied rigorously by methods independent of machine learning [Zub23], [LOP25], [BLLSZ24]. At the time of discovery, it was noted heuristically that the murmururation patterns associated with a dataset of elliptic curves appear correlated with the weightings in the first principal component of that dataset [HLOP24]. This suggests, perhaps counterintuitively, that when elliptic curves with conductor in a fixed interval are separated by rank using principal component analysis, the Frobenius traces at certain primes contribute more significantly than others. Subsequently, Pozdnyakov observed murmurations by applying interpretability techniques to convolutional neural networks trained to predict analytic rank, more precisely, by analyzing their learned convolutional filters [Poz24]. At the same time, Pozdnyakov observed that

---

*Date:* March 19, 2026.

Mestre–Nagao sums also contribute to rank predictions, which is perhaps unsurprising since they are expected to converge to a value closely connected to the rank, and they have historically played a significant role in the discovery of elliptic curves with high rank [EK20]. In contrast to the oscillating feature importance suggested by murmurations, Mestre–Nagao sums weight primes up to a fixed bound, with feature importance decaying on the order of  $\log(p)/p$ . On the other hand, in keeping with the observation that certain primes may be more pertinent than others to rank prediction, it has been observed that Mestre–Nagao sums up to smaller bounds can sometimes yield more accurate predictions than those up to larger ones, and that the numerical discrepancy can be attributed to murmurations [BKN24].

In this paper, we apply a different interpretability technique to a CNN trained to predict analytic rank on a larger dataset of elliptic curves. We reproduce earlier observations that both murmurations and Mestre–Nagao sums influence rank predictions for elliptic curves made by convolutional neural networks (CNNs). We then extend this analysis by systematically investigating their relative impact. Whereas Pozdnyakov analyzes binned averages of  $a_p$  (which amplifies the impact of murmurations), we are able to examine the individual values. This constitutes our first main contribution. Our primary tool is the study of *saliency* curves for the CNNs, which are analogous to the principal component weightings considered in [HLOP24], but contrast with the convolutional filters analyzed in [Poz24]. The evolution of these saliency curves reveals how the balance between murmurations and Mestre–Nagao sums changes over the course of training. In early epochs, the saliency curves exhibit clear murmurations-like patterns, whereas in later epochs the importance of primes decays in a manner closely resembling the Mestre–Nagao weightings.

As our next main contribution, we examine how the conductor affects this balance. In particular, we show experimentally that murmurations play a substantially larger role in rank prediction for curves with smaller conductor than for those with larger conductor. More generally, the contribution of murmurations depends on several factors, including the training epoch, the conductor range, and the rank itself. For example, even for datasets with small conductor and in early epochs, murmurations-like patterns persist only in the saliency curves associated with rank 1, and do not appear for curves of rank  $> 1$ .

We conclude this introduction with an overview of the following sections. In Section 2, we describe our datasets and the architecture of our CNN, report high prediction accuracy, and investigate how the accuracy depends on the number of primes. In Section 3, we present the saliency curves and explore the interplay among predicted rank, murmurations, Mestre–Nagao sums, and conductor ranges.

**Acknowledgments.** We thank Alexey Pozdnyakov for helpful discussions. We also thank the Harvard University Center of Mathematical Sciences and Applications and, in particular, the organizers and attendees of the Mathematics and Machine Learning Program from 2024 and the Reunion from 2025. This collaboration grew out of these programs. Costa was supported by Simons Foundation grant SFI-MPS-Infrastructure-00008651. Qi was supported by the NSF grant PHY-2019786 (the NSF AI Institute for Artificial Intelligence and Fundamental Interactions).

## 2. DATA, ARCHITECTURE, AND ACCURACY

In this section, we seek to predict the rank of elliptic curves using one-dimensional CNNs. We specify our dataset in Section 2.1 and our CNN architecture in Section 2.2. We achieve accuracy comparable to that in [KV23] and [Poz24], and record how the accuracy varies with the number of Frobenius traces used to represent the data points.

**2.1. Data specification.** Let  $E$  be an elliptic curve over  $\mathbb{Q}$ . If  $p$  is a good prime for  $E$ , then we define  $a_p(E) := p + 1 - \#E(\mathbb{F}_p)$ . If  $p$  is a bad prime for  $E$ , then  $a_p(E) \in \{-1, 0, 1\}$  is defined according to the reduction type for  $E \bmod p$  [Sil94]. The *conductor* of  $E$  is a positive integer whose prime divisors are precisely the bad primes, with exponents determined by the reduction type at each such prime [Sil09]. Roughly speaking, the conductor measures the arithmetic complexity of the elliptic curve. According to the Hasse bound, for a prime  $p$ , we may normalise  $a_p$  as follows:

$$\tilde{a}_p(E) = \frac{a_p(E)}{2\sqrt{p}} \in [-1, 1].$$

In this section, we will use a dataset called **XECQ**, which contains 1,536,784 elliptic curves over  $\mathbb{Q}$  with conductor no greater than 400,000 (**XECQ** is a subset of the larger set, available at [C25]). Each elliptic curve in **XECQ** has (analytic) rank in the set  $\{0, 1, 2, 3, 4\}$ . We represent each datapoint  $E$  in **XECQ** by a vector of the form:

$$(2.1) \quad v_E = (\tilde{a}_p(E))_{p \leq b} \in [-1, 1]^{\pi(b)},$$

where  $b \in \mathbb{Z}_{>0}$  and  $\pi(b)$  denotes the number of primes  $\leq b$ . While we occasionally allow  $b$  to vary, we fix  $b = 10,000$  for the most part, so that  $\pi(b) = 1,229$ . The distribution of conductors within **XECQ** is shown in Figure 2.1. For an interval  $[A, B] \subset \mathbb{R}_{>0}$ , we denote by **XECQ**[ $A, B$ ] the subset of **XECQ** containing only curves with conductor in  $[A, B]$ . In Table 2.1, we display four choices of intervals  $[A, B]$  that yield approximately the same number of data points in **XECQ**[ $A, B$ ].

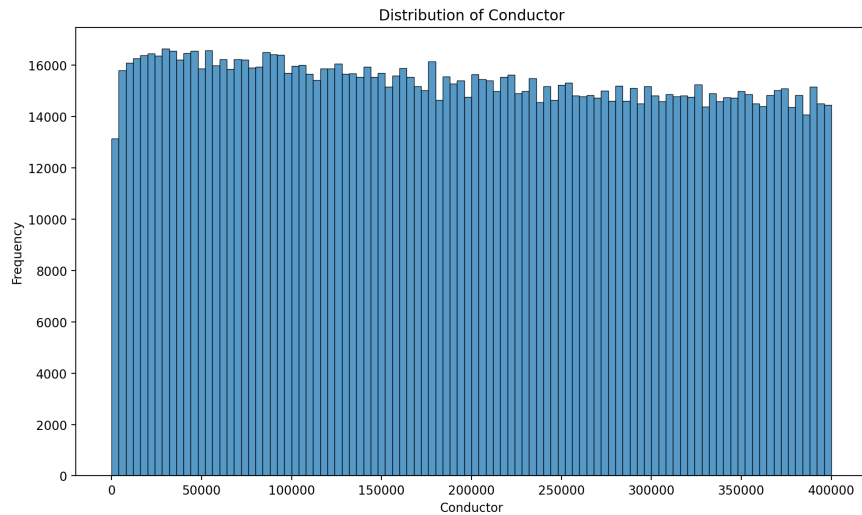


FIGURE 2.1. Distribution of conductors in **XECQ**.

$[A, B]$	$\#\text{XECQ}[A, B]$
$[0, 10000]$	36,838
$[100000, 110000]$	39,667
$[200000, 210000]$	38,905
$[300000, 310000]$	36,742

TABLE 2.1. Number of elliptic curves in **XECQ** with conductor in the specified interval.

**2.2. Architecture and accuracy.** The code used for the experiments described in this paper is available at [Qi26]. For each of the four intervals  $[A, B]$  listed in Table 2.1, we split  $\text{XECQ}[A, B]$  into training and test sets using an 80:20 ratio and train a one-dimensional convolutional neural network (1D CNN) to predict the rank. The architecture of our neural network is summarised in Table 2.2. In particular, the network consists of three 1D convolutional layers, with 16, 32 and 64 channels respectively, each using kernel size  $K = 3$  and padding  $P = 1$ . Each convolutional layer is followed by a ReLU activation function, and a max-pooling layer with  $K = 2$  and  $P = 1$ . After a dropout layer with  $D = 0.5$ , the convolutional blocks are followed by two fully connected layers with 128 neurons each, and a final output layer with width 5 (that is, the number of possible vanishing orders in **XECQ**). The network is trained with cross-entropy loss using the Adam optimizer, with batch size 3,000 and learning rate 0.001. Each epoch consists of ten steps based on the chosen mini-batch size.

Layer (Type)	Output Shape	Param #
Conv1D	$[1, 16, 1229]$	64
MaxPool1D	$[1, 16, 615]$	–
Conv1D	$[1, 32, 615]$	1,568
MaxPool1D	$[1, 32, 308]$	–
Conv1D	$[1, 64, 308]$	6,208
MaxPool1D	$[1, 64, 155]$	–
Flatten & Dropout	$[1, 9920]$	–
Linear	$[1, 128]$	1,269,888
Linear	$[1, 128]$	16,512
Linear	$[1, 4]$	516
Total Trainable Parameters		1,294,756

TABLE 2.2. Architecture summary of the 1D CNN.

In summary, our model is a shallow, fixed-depth architecture that progressively increases the number of channels, applies max-pooling, incorporates fully connected layers, and uses explicit dropout regularization. In contrast, the CNN of [KV23] is a modular, fully convolutional architecture that increases the number of channels only once, employs strided convolutions for downsampling in dedicated layers, and preserves feature dimensions elsewhere. For larger-scale experiments, Pozdnyakov adopts a similar architecture to that of [KV23], as described in [Poz24, Section 4.2].

In Table 2.3, we report the best observed accuracy for each conductor interval  $[A, B]$ . As in [KV23] and [Poz24], we observe high predictive accuracy. Figure 2.2 displays the prediction

$[A, B]$	best observed accuracy
$[0, 10000]$	99.85%
$[100000, 110000]$	99.22%
$[200000, 210000]$	99.07%
$[300000, 310000]$	98.57%

TABLE 2.3. Best observed accuracy for the 1D CNN described in 2.2 when applied to  $\mathbf{XECQ}[A,B]$

accuracy of each CNN as a function of the number of training epochs. It is generally expected that curves with larger conductor are more arithmetically complex and therefore may require more information to achieve the same level of accuracy in rank prediction. With this in mind, the left (resp. right) panel of Figure 2.3 plots the prediction accuracy as a function of  $\pi(b)$  (resp.  $\log \pi(b)$ ), that is, the number of features (resp. its logarithm).

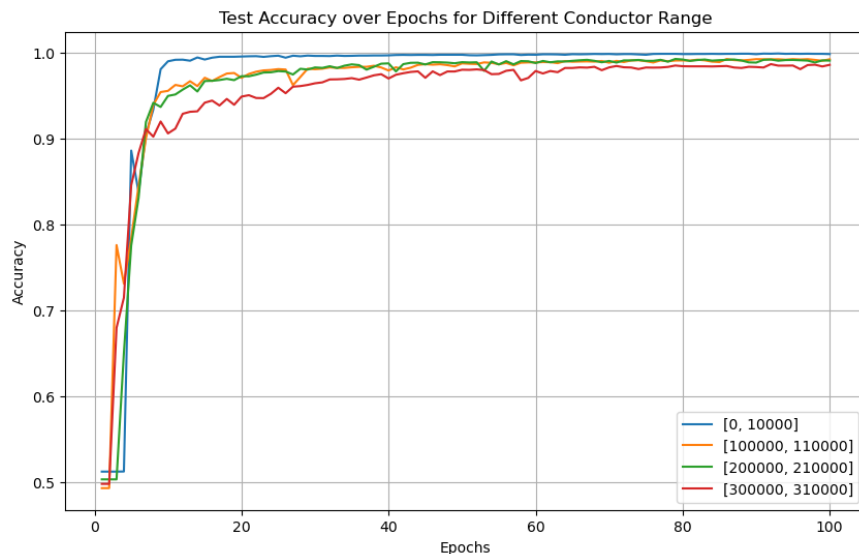


FIGURE 2.2. Learning the rank in  $\mathbf{XECQ}[A,B]$ : percentage accuracy against epoch. Each colour corresponds to one of the 4 conductor intervals specified.

### 3. SALIENCY CURVES

To interpret the predictions of the CNN from Section 2.2, we analyze the feature importance using saliency scores. In [Poz24], two key influences on analytic rank prediction are identified: murmurations and Mestre–Nagao sums. In this section, we will observe that the relative contributions of these factors vary depending on the predicted rank, the conductor range, and the training stage.

3.1. **Definitions.** After each epoch, the CNN from Section 2.2 determines a function

$$(3.1) \quad [-1, 1]^{\pi(b)} \rightarrow \{0, 1, 2, 3, 4\},$$

which assigns to each input vector  $(x_q)_{q \leq b}$ , with  $x_q \in [-1, 1]$  for primes  $q \leq b$ , a predicted class (that is, predicted rank). Although the function in (3.1) depends on the epoch, we will suppress

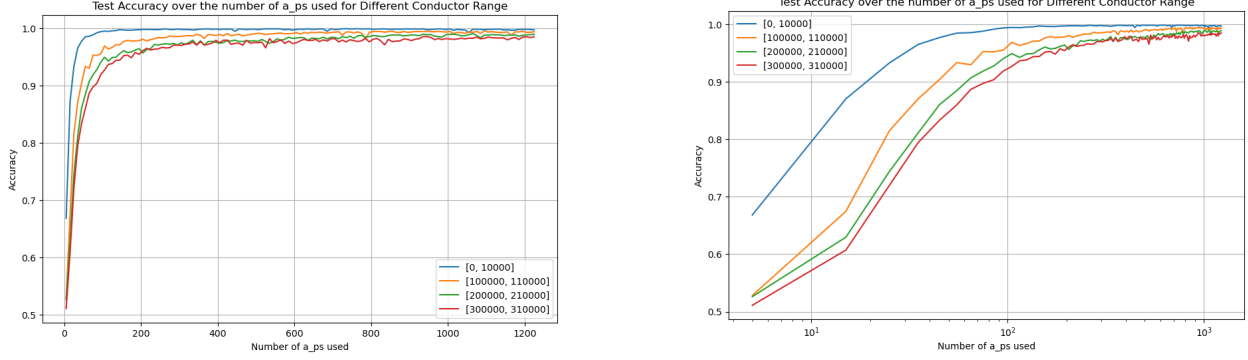


FIGURE 2.3. Learning the rank in  $\text{XECQ}[A,B]$ : (Left) test accuracy against number of primes used in training for different choices of  $[A, B]$ . (Right) test accuracy against the logarithm of the number of primes used in training for different choices of  $[A, B]$ .

this from subsequent notation. The function in equation (3.1) factors through a map

$$S : [-1, 1]^{\pi(b)} \longrightarrow \mathbb{R}^5,$$

$$S((x_q)_{q \leq b}) = (S_0, S_1, S_2, S_3, S_4),$$

where, for each class  $v \in \{0, 1, 2, 3, 4\}$ , the quantity  $S_v$  denotes the score assigned to the input. The probability that a given input  $\mathbf{x} := (x_q)_{q \leq b} \in [-1, 1]^{\pi(b)}$  belongs to class  $v$  is then defined by the softmax function

$$P_v(\mathbf{x}) = \frac{e^{S_v}}{\sum_{i=0}^4 e^{S_i}},$$

where  $v \in \{0, 1, 2, 3, 4\}$ . The predicted class of the input  $\mathbf{x}$  is given by

$$c(\mathbf{x}) = \operatorname{argmax}_{v \in \{0,1,2,3,4\}} P_v(\mathbf{x}).$$

Consider a class  $v$  and an input  $\mathbf{x} = (x_q)_{q \leq b} \in [-1, 1]^{\pi(b)}$ . For a prime  $p \leq b$ , define the *saliency score*  $w_p^v(\mathbf{x})$  to be the derivative of  $S_v$  with respect to  $x_p$  at  $\mathbf{x} \in [-1, 1]^{\pi(b)}$ :

$$(3.2) \quad w_p^v(\mathbf{x}) = \frac{\partial S_v(\mathbf{x})}{\partial x_p}, \quad p \leq b.$$

Applying a first-order Taylor expansion to  $S_v$  around  $\mathbf{x}$ , then evaluating at  $\mathbf{0}$  gives:

$$(3.3) \quad S_v(\mathbf{0}) \approx S_v(\mathbf{x}) + \sum_{p \leq b} w_p^v(\mathbf{x}) (0 - x_p).$$

Subsequently, we obtain

$$(3.4) \quad S_v(\mathbf{x}) \approx S_v(\mathbf{0}) + \sum_{p \leq b} w_p^v(\mathbf{x}) x_p.$$

Let  $E$  be an elliptic curve over  $\mathbb{Q}$ . After setting  $\mathbf{x} = (\tilde{a}_p(E))_{p \leq b}$ , equation (3.4) suggests that the saliency scores  $w_p^v(\mathbf{0})$  can be viewed as somewhat analogous to the weights in the Mestre–Nagao sum:

$$(3.5) \quad \frac{1}{\log(b)} \sum_{p \leq b} \frac{\log(p)}{p} a_p(E) = \frac{2}{\log(b)} \sum_{p \leq b} \frac{\log(p)}{\sqrt{p}} \tilde{a}_p(E), \quad b \in \mathbb{R}.$$

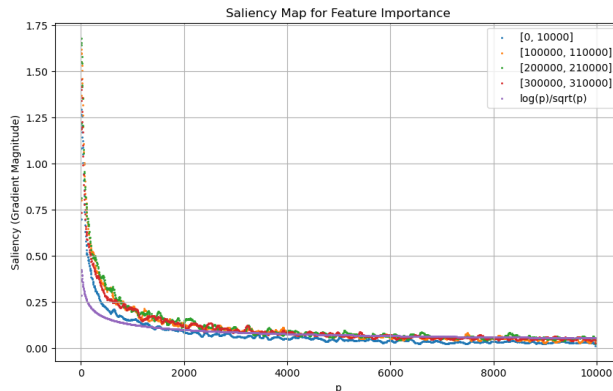


FIGURE 3.1. Comparison of the saliency scores  $w_p$  with the Mestre–Nagao weighting. In this figure, the saliency scores are computed after 100 epochs.

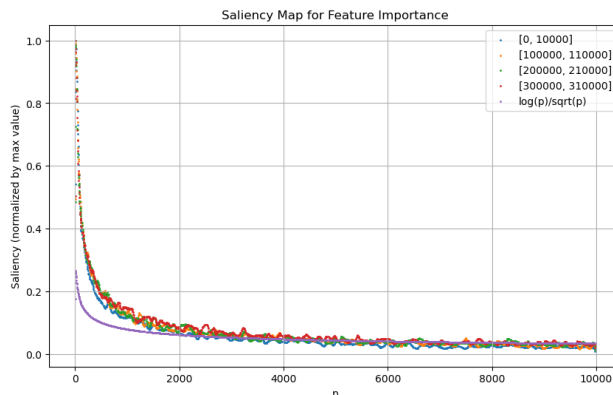


FIGURE 3.2. Comparison the normalized saliency scores  $\tilde{w}_p$  with the Mestre–Nagao weighting. In this figure, the normalised saliency scores are computed after 100 epochs.

Our next intention is to visualise averaged saliency scores. By doing that, we are able to observe a visual comparison with Mestre–Nagao sums and interpret the CNN predictions.

**3.2. Visualisation and interpretation.** For an interval  $[A, B] \subset \mathbb{R}$ , we denote by  $\text{XECQ}^\circ[A, B]$  a test subset of  $\text{XECQ}[A, B]$  and, for  $v \in \{0, 1, 2, 3, 4\}$ , we let  $\text{XECQ}^\circ[A, B|v]$  be the subset of  $\text{XECQ}^\circ[A, B]$  with predicted rank  $v$ . For  $E \in \text{XECQ}^\circ[A, B]$ , we take  $\mathbf{x} = (\tilde{a}_q(E))_{q \leq b}$  in equation (3.2) and write  $w_p^v(E) := w_p^v(\mathbf{x})$  to indicate that  $\mathbf{x} = (\tilde{a}_q(E))_{q \leq b}$  is determined by  $E$ .

For each prime  $p \leq b$ , define

$$(3.6) \quad w_p := \frac{1}{\#\text{XECQ}^\circ[A, B]} \sum_{v \in \{0, 1, 2, 3, 4\}} \sum_{E \in \text{XECQ}^\circ[A, B|v]} |w_p^v(E)|,$$

and also consider the following normalisation of  $w_p$ :

$$\tilde{w}_p = \frac{w_p}{\max\{w_q : q \leq b, q \text{ prime}\}} \in [0, 1].$$

In Figure 3.1 (resp. Figure 3.2) we plot  $w_p$  (resp.  $\tilde{w}_p$ ) and  $\log(p)/\sqrt{p}$ , that is, the coefficient for  $\tilde{a}_p(E)$  in equation (3.5).

The averaged saliency score in equation (3.6) sums over all possible ranks in order to compare with the Mestre–Nagao weightings, which are the same for every curve, irrespective of its analytic rank.

In order to interpret the predictions made by the CNN, we need to understand the saliency of each class. To that end, for  $v \in \{0, 1, 2, 3, 4\}$ , we define

$$(3.7) \quad W_p^v := \frac{1}{\#\text{XECQ}^\circ[A, B|v]} \sum_{E \in \text{XECQ}^\circ[A, B|v]} w_p^v(E).$$

It is conventional to take the absolute value of the saliency scores (as in equation (3.6)), however the sign is perhaps interesting from an arithmetic perspective and so we not do that in equation (3.7). That being said, for each  $v \in \{0, 1, 2, 3, 4\}$ , we normalize  $W_p^v$  as follows:

$$\widetilde{W}_p^v = \frac{W_p^v}{\max\{|W_q^v|: q \leq b, q \text{ prime}\}} \in [-1, 1],$$

in which the denominator does utilise an absolute value. Plotting  $p$  against  $\widetilde{W}_p^v$  after epoch yields the so-called *saliency curve* for  $v$ . These curves highlight which primes the network deems most important for its predictions.

Figures 3.3, 3.4, 3.5 and 3.6 show several saliency curves for the conductor intervals in Table 2.1 (see Conventions 3.1 for the common features of the figures). We observe that the saliency curves exhibit notable differences across conductor intervals  $[A, B]$ , ranks  $v$ , and training stages. For each conductor interval, all curves are predicted to have rank 1 at the first epoch (note that, at the first epoch, no plots appear for the other ranks because the corresponding sets  $\text{XECQ}^\circ[A, B|v]$  are empty). By the second epoch, some curves are predicted to have rank 0, and higher-rank predictions appear at later epochs.

For  $[A, B] = [0, 10000]$ , Figure 3.3 shows that the curves for  $v = 0$  (blue) and  $v = 1$  (orange) develop opposite signs within the first few epochs. From epoch 2 onward, their peaks align with those seen in the murmuration phenomenon of [HLOP24]. This indicates that the CNN exploits murmurations to distinguish between ranks 0 and 1 during the early stages of training. Remarkably, this behavior emerges even though there is no visible murmuration in the average value of  $\tilde{a}_p$  [Sut22], suggesting that the CNN is able to identify the hidden pattern in the dataset. As training progresses, the saliency curve for rank 0 (blue) gradually flattens and places increasing emphasis on smaller primes, resembling the Mestre–Nagao weightings in equation (3.5). In addition, a saliency curve for  $v = 2$  (green) appears, resembling the shape of the curve for  $v = 0$  but with the opposite sign. These observations align with the pattern from [HLOP24, Figure 1], where rank 1 is distinguished by the murmuration, and ranks 0 and 2 are separated mainly by the smaller primes.

For the larger conductor intervals shown in Figures 3.4, 3.5, and 3.6, the influence of murmuration appears to diminish, and the CNN relies primarily on smaller primes for classification, again in a manner consistent with the Mestre–Nagao weightings.

**Conventions 3.1.** Figures 3.3–3.6 share the same conventions: Each epoch consists of 10 steps (or batches). The plots display the results from step 0 only. Each color corresponds to a different predicted rank. At the first and second epochs, no plots appear for ranks other than 1, since all curves are predicted to have rank 1. The saliency scores are normalized so that their maximum value is equal to 1.

**3.3. Check with synthetic data.** To further investigate what CNN has learned, we conducted an experiment using synthetic data. Use of synthetic data was adopted in [HLO22b], to which we refer the reader for the discussion of the Sato–Tate distribution of  $(a_p)_p$ . We generated a dataset of 500,000 sequences  $(a_p)_p$  by drawing each coefficient independently from the Sato–Tate distribution, thereby producing data that mimics the statistical behaviour of elliptic  $L$ -functions but is highly unlikely to arise from an elliptic curve in our dataset. It is possible to identify each synthetic datapoint with some elliptic curve of large height and, therefore, most likely of much larger conductor. We then fed these synthetic sequences into the CNN trained on XECQ with conductor range  $[0, 10000]$  and recorded the predicted rank for each sequence. Finally, we grouped the synthetic curves by their predicted rank and computed the average unnormalized  $a_p$  within each group. The results are shown in Figure 3.7. Remarkably, the average  $a_p$  for sequences predicted to be rank 0, 1 and 2 exhibit a clear separation, which resembles the divergence observed in real data. This confirms that the CNN has learned to associate specific bias patterns in the  $a_p$ ’s with the rank.

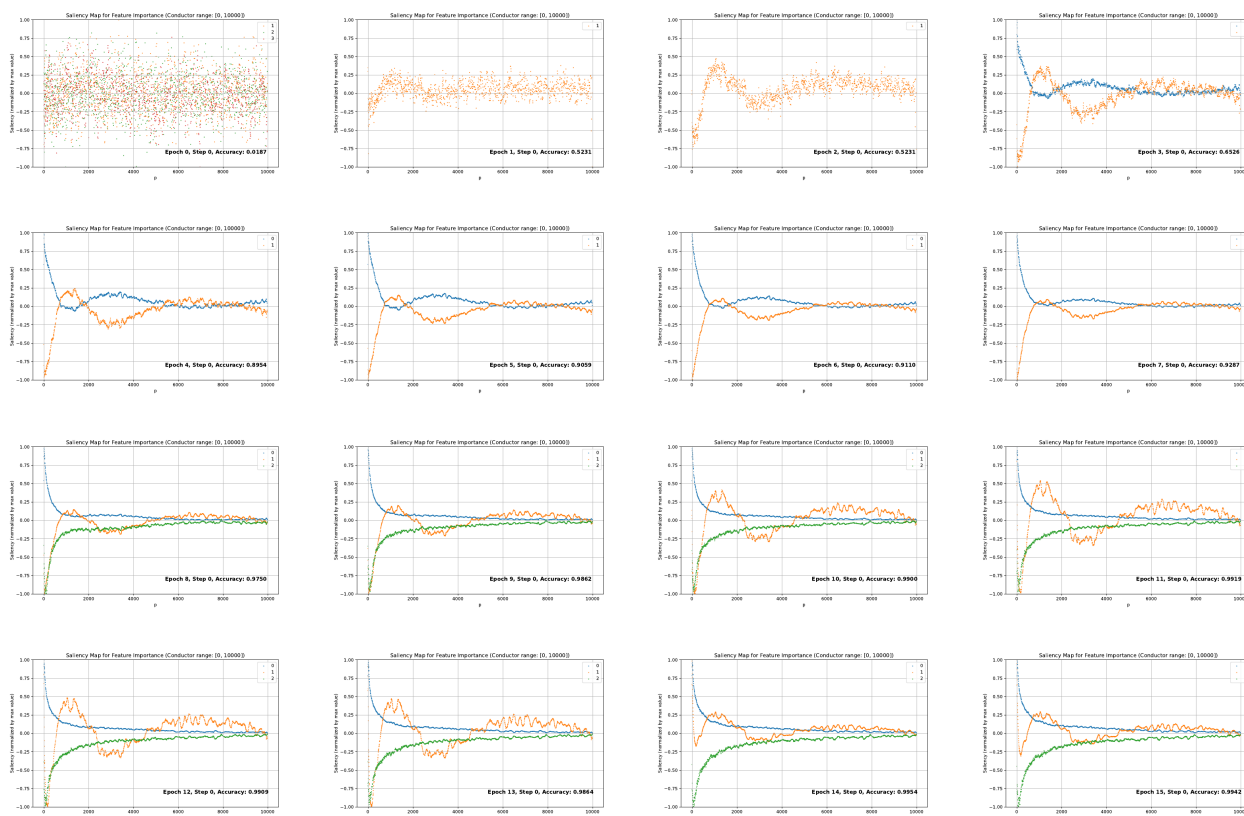


FIGURE 3.3. Evolution of saliency scores over the epochs for XECQ[0, 10000]. See Conventions 3.1 for the conventions of the figure.

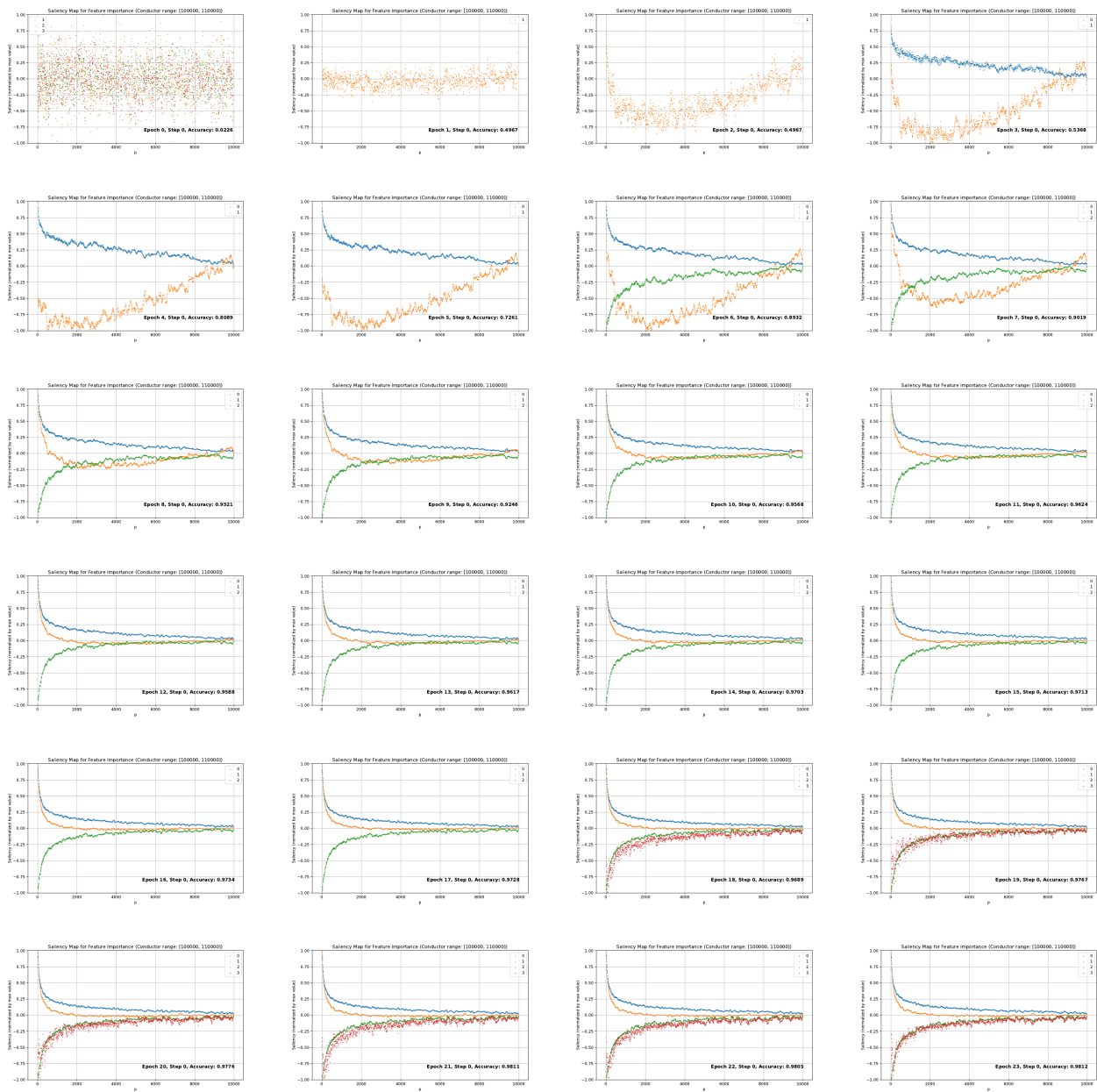


FIGURE 3.4. Evolution of saliency scores over the epochs for conductor interval [100000, 110000]. See Conventions 3.1 for the conventions of the figure.

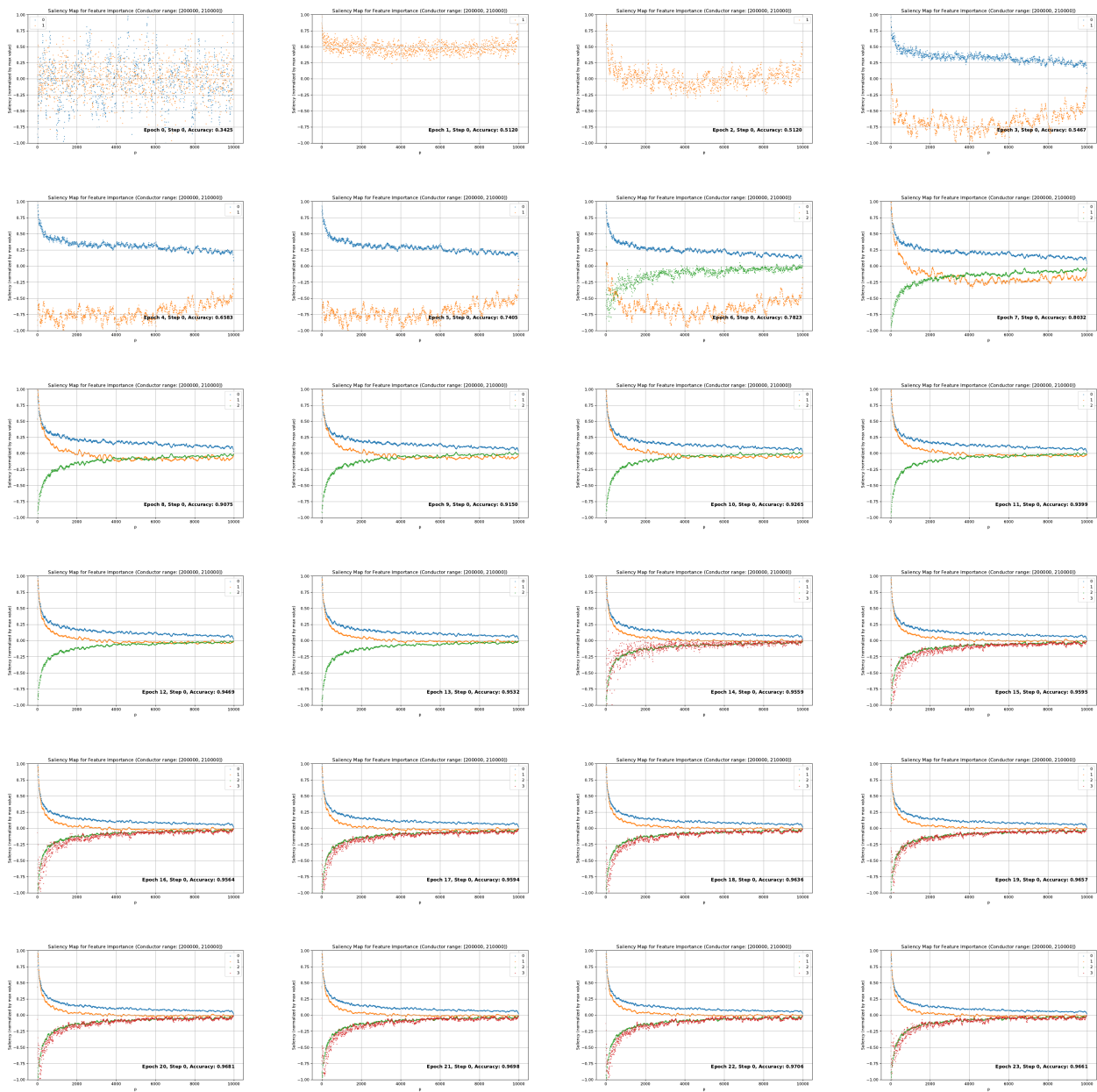


FIGURE 3.5. Evolution of saliency scores over the epochs for conductor interval [200000, 210000]. See Conventions 3.1 for the conventions of the figure.

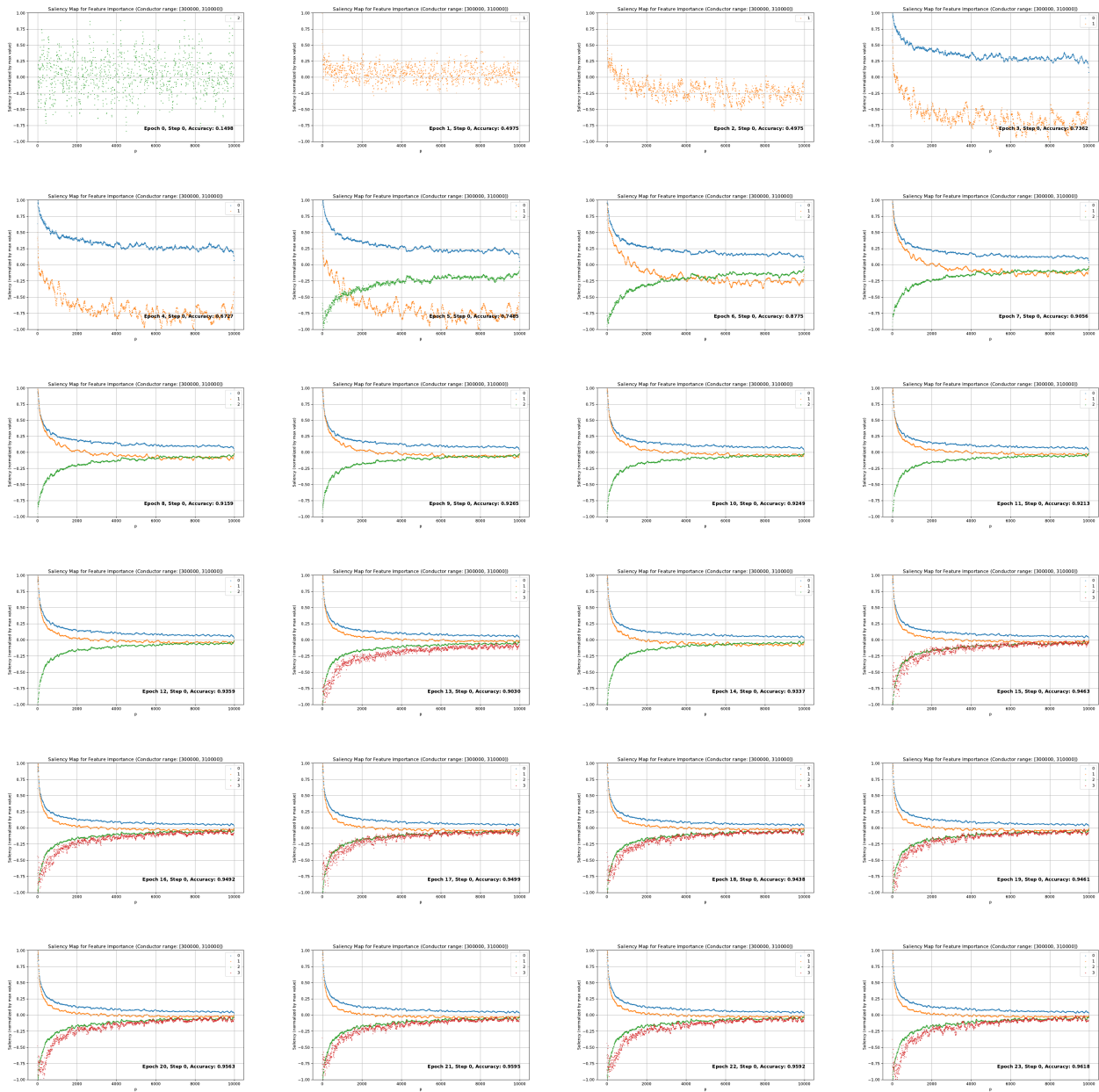


FIGURE 3.6. Evolution of saliency scores over the epochs for conductor interval [300000, 310000]. See Conventions 3.1 for the conventions of the figure.

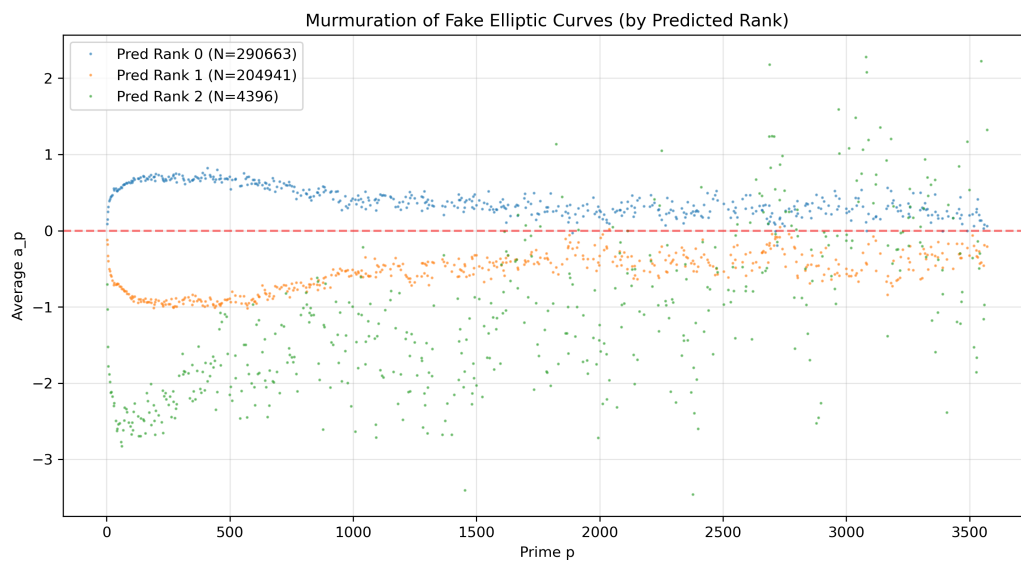


FIGURE 3.7. Average values of  $a_p$  (unnormalized) for the synthetic data, grouped by the rank predicted by the CNN. The network produces a clear separation between the predicted classes.

## REFERENCES

- [AHLOS23] Malik Amir, Yang-Hui He, Kyu-Hwan Lee, Thomas Oliver, and Eldar Sultanow. “Machine-learning of the class number of real quadratic fields”. In: *International Journal of Data Science in the Mathematical Sciences* 1(2) (2023), pp. 107–134 (↑ 1).
- [BBFHS24] Angelica Babei, Barinder S. Banwait, AJ Fong, Xiaoyu Huang, and Deependra Singh. “Machine Learning Approaches to the Shafarevich-Tate Group of Elliptic Curves”. [arXiv:2508.06670](https://arxiv.org/abs/2508.06670). 2024 (↑ 1).
- [BBCDLLQV25a] J. Bieri, G. Butbaia, E. Costa, A. Deines, K.-H. Lee, D Lowry-Duda, T. Oliver, Y. Qi, and T. Veenstra. “Learning Fricke signs from Maass form Coefficients”. <https://arxiv.org/abs/2501.02105>. arXiv: math.NT: 2501.02105. 2025 (↑ 1).
- [BBCDLLQV25b] J. Bieri, G. Butbaia, E. Costa, A. Deines, K.-H. Lee, D Lowry-Duda, T. Oliver, Y. Qi, and T. Veenstra. “Machine learning the vanishing order of rational  $L$ -functions”. <http://arxiv.org/abs/2502.10360v1>. arXiv: math.NT: 2502.10360. 2025 (↑ 1).
- [BLLSZ24] Andrew R. Booker, Min Lee, David Lowry-Duda, Andrei Seymour-Howell, and Nina Zubrilina. “Murmurations of Maass forms”. [arXiv:2409.00765](https://arxiv.org/abs/2409.00765). 2024 (↑ 1).
- [BKN24] Zvonimir Bujanović, Matija Kazalicki, and Lukas Novak. “Murmurations of Mestre-Nagao sums”. <http://arxiv.org/abs/2403.17626v1>. arXiv: math.NT: 2403.17626v1. 2024 (↑ 2).
- [C25] Edgar Costa. “Frobenious traces for a set of isogeny classes of elliptic curves of conductor up to  $10^6$ ”. <https://zenodo.org/records/15777475>. 2025 (↑ 3).
- [EK20] N. Elkies and Z. Klagsbrun. “New Rank Records For Elliptic Curves Having Rational Torsion”. <http://arxiv.org/abs/2003.00077>. arXiv: math.NT: 2003.00077. 2020 (↑ 2).
- [HLO22a] Yang-Hui He, Kyu-Hwan Lee, and Thomas Oliver. “Machine-learning number fields”. In: *Math. Comput. Geom. Data* 2.1 (2022), pp. 49–66 (↑ 1).
- [HLO22b] Yang-Hui He, Kyu-Hwan Lee, and Thomas Oliver. “Machine-learning the Sato-Tate conjecture”. In: *J. Symbolic Comput.* 111 (2022), pp. 61–72 (↑ 9).
- [HLO23] Yang-Hui He, Kyu-Hwan Lee, and Thomas Oliver. “Machine learning invariants of arithmetic curves”. In: *J. Symbolic Comput.* 115 (2023), pp. 478–491 (↑ 1).
- [HLOP24] Yang-Hui He, Kyu-Hwan Lee, Thomas Oliver, and Alexey Pozdnyakov. “Murmurations of Elliptic Curves”. In: *Experimental Mathematics* (2024), pp. 1–13 (↑ 1, 2, 8).
- [KV23] Matija Kazalicki and Domagoj Vlah. “Ranks of elliptic curves and deep neural networks”. In: *Res. Number Theory* 9.3 (2023), Paper No. 53, 21 (↑ 1, 3, 4).
- [LL24] Kyu-Hwan Lee and Seewoo Lee. “Machines Learn Number Fields, But How? The Case of Galois Groups”. [arXiv:2508.06670](https://arxiv.org/abs/2508.06670). 2024 (↑ 1).
- [LOP25] Kyu-Hwan Lee, Thomas Oliver, and Alexey Pozdnyakov. “Murmurations of Dirichlet Characters”. In: *Int. Math. Res. Not. IMRN* 1 (2025), rnae277 (↑ 1).

- [Poz24] Alexey Pozdnyakov. “Predicting root numbers with neural networks”. <http://arxiv.org/abs/2403.14631v1>. arXiv:math.NT:2403.14631v1. 2024 (↑ 1, 2, 3, 4, 5).
- [Qi26] Yidi Qi. “Murmurations-cnn”. <https://github.com/yidiq7/murmurations-cnn>. 2026 (↑ 4).
- [Sil94] J. H. Silverman. “Advanced topics in the arithmetic of elliptic curves”. Springer Science & Media, 1994 (↑ 3).
- [Sil09] Joseph H. Silverman. “The Arithmetic of Elliptic Curves”. Vol. 106. Graduate Texts in Mathematics. Dordrecht: Springer, 2009 (↑ 3).
- [Sut22] Andrew Sutherland. “Letter from Sutherland to Rubinstein and Sarnak”. <https://math.mit.edu/~drew/RubinsteinSarnakLetter.pdf>. 2022 (↑ 8).
- [Zub23] Nina Zubrilina. “Murmurations”. arXiv:2310.07681. 2023 (↑ 1).

UNIVERSITY OF REDLANDS, REDLANDS, CA 92373, USA

*Email address:* [joanna.bieri@redlands.edu](mailto:joanna.bieri@redlands.edu)

DEPARTMENT OF MATHEMATICS, MASSACHUSETTS INSTITUTE OF TECHNOLOGY, CAMBRIDGE, MA 02139, USA

*Email address:* [edgarc@mit.edu](mailto:edgarc@mit.edu)

*URL:* <https://edgarcosta.org>

CENTER FOR COMMUNICATIONS RESEARCH, LA JOLLA, USA

*Email address:* [aly.deines@gmail.com](mailto:aly.deines@gmail.com)

DEPARTMENT OF MATHEMATICS, UNIVERSITY OF CONNECTICUT, STORRS, CT 06269, USA

KOREA INSTITUTE FOR ADVANCED STUDY, SEOUL 02455, REPUBLIC OF KOREA

*Email address:* [khlee@math.uconn.edu](mailto:khlee@math.uconn.edu)

ICERM, PROVIDENCE, RI, 02903, USA

DEPARTMENT OF MATHEMATICS, BROWN UNIVERSITY, PROVIDENCE, RI, 02912, USA

*Email address:* [david@lowryduda.com](mailto:david@lowryduda.com)

*URL:* <https://davidlowryduda.com>

UNIVERSITY OF WESTMINSTER, LONDON, UK

*Email address:* [T.Oliver@westminster.ac.uk](mailto:T.Oliver@westminster.ac.uk)

DEPARTMENT OF PHYSICS, NORTHEASTERN UNIVERSITY, BOSTON, MA, USA

NSF INSTITUTE FOR ARTIFICIAL INTELLIGENCE AND FUNDAMENTAL INTERACTIONS, CAMBRIDGE, MA, USA

*Email address:* [y.qi@northeastern.edu](mailto:y.qi@northeastern.edu)

CENTER FOR COMMUNICATIONS RESEARCH, LA JOLLA, USA

*Email address:* [tamarabveenstra@gmail.com](mailto:tamarabveenstra@gmail.com)